

Scientific accomplishments 2021

The DEPSIS project is embedded as part of the CERN-RD50 efforts, with a team of 7 scientists (1 MS student, 1 PhD student, 2 PostDocs, 3 senior researchers) and 2 technicians. The scientific motivation of the project is the need for improving the radiation hardness of different types of p-type silicon sensors (single pads, pixel and strips, LGAD and HVCMOS) to be used in ATLAS and CMS Strip Tracker upgrades for HL-LHC, and the defect engineering is our key strategy for this purpose. In Boron doped p-type silicon the most obvious change observed in the electrical performance is the loose of the doping due to irradiation, due to reaction between substitutional Boron (B_s) with Silicon interstitials (Si_i) created by irradiation, that change the position of B from the substitutional to an interstitial site, becoming thus electrically inactive. The project focusses on investigation of generation and kinetics of isolated point defects and clusters induced by irradiation with different particles in defect engineered p-type silicon in order to understand the formation of impurity related radiation induced defects and provide solutions for controlling the “acceptor removal” process in the envisaged sensors. Systematic studies were performed on a serie of Si diodes processed on defect engineered Si, obtained by epitaxial growth of a 45 μm thick layer of Si on 10 Ωcm Cz substrates. Diodes of different resistivities, of 10, 50, 250 and 1000 Ωcm , all having the same amount of C and O impurities were investigated. CZ and FZ diodes of 100 and 1000 Ωcm resistivity, were also studied in comparison with EPI diodes after irradiation with 23 GeV protons and 1 MeV neutrons, fluences between 10^{10} and 10^{19} cm^{-2} .

The original and novel results obtained according to each type of investigation performed (Ax) are:

A1) Analyses of impurity content. Unirradiated samples were first investigated by spectroscopic techniques in order to determine the amount of C, O and B in the investigated diodes. The amount of C in EPI and CZ materials is $\sim 1.3 \times 10^{16}$ cm^{-3} and in FZ is close to the detection limit $\sim 10^{15}$ cm^{-3} . The B content could be detected by SIMS only in the low resistivity CZ substrate of the epilayers, in the order of 2×10^{18} cm^{-3} . By the use of the newly installed LA-ICPMS in NIMP it became possible to detect B in low concentration, however, only after developing of *proper calibration standards inhouse*. LA-ICPMS results revealed a significant larger than expected amount of B in the diodes, as well as significant concentration of P. This means that the doping in medium and high resistivity p-type diodes was achieved by compensation between B and P dopants and *the Boron content can not be anymore assimilated with the doping concentration*, as determined from C-V curves of non-irradiated diodes.

A2) TEM investigations – annealing at temperatures 80÷350 °C. For microstructural investigations the JEOL 2100 TEM has been used. LGAD samples irradiated with up to 10^{19} n/cm^2 have been prepared using the conventional cross-section method based on mechanical thinning and Ar ion polishing. *A linear pattern of point defects is observed in the first tens of nm beyond the interface, on the [001] crystalline direction – see Fig.1.* The linear pattern of the defects is observed on the [001] crystalline direction and no changes occurred during annealing at 80 °C. Strain maps show very low magnitudes with no changes during the annealing at 80 C. *These well defined tracks of point defects (vacancies and/or interstitials) or very small clusters of point defects remain also after treatment at elevated temperatures.* In addition, starting from 200 °C, significantly larger clusters of defects start to form – see Fig.2. Notably, *the silicon remains crystalline even after such extreme irradiation of 10^{19} n/cm^2 .*

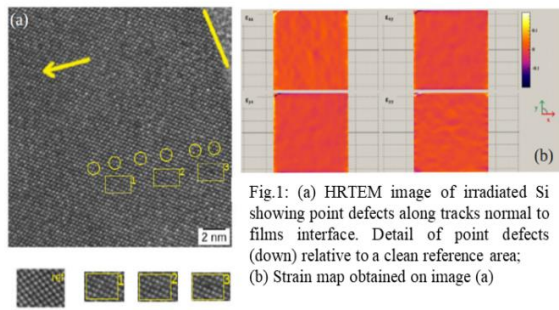


Fig.1: (a) HRTEM image of irradiated Si showing point defects along tracks normal to films interface. Detail of point defects (down) relative to a clean reference area; (b) Strain map obtained on image (a)

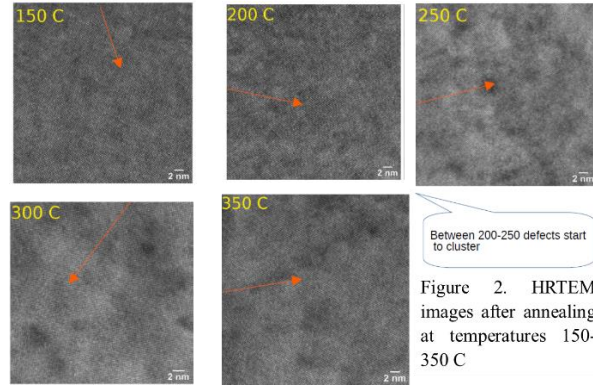


Figure 2. HRTEM images after annealing at temperatures 150-350 C

A3) Electrical characterization and subsequent data analysis and modelling (CV, IV, DLTS and TSC)

- detection and electrical characterization of all the defects induced by irradiation, determine the defect generation rate(s) and the role of impurities in their formation, evaluate the impact on the acceptor removal rate (e.g. B_iO_i defect), time evolution. *Four new holes traps were detected, of which only 2 could be well separated and full characterized: H156K ($\sigma_h=4.8 \times 10^{-16} \text{ cm}^2$, $E_a=0.29 \text{ eV}$) and H223K ($\sigma_h=1.7 \times 10^{-17} \text{ cm}^2$, $E_a=0.36 \text{ eV}$).*

- Electrical properties of the B_iO_i defect and its generation rate(s)- DLTS: field dependent E_a and determination of both capture cross sections for electrons and holes ($E_a=0.24-0.25 \text{ eV}$, $\sigma_e = 1 \times 10^{-14} \text{ cm}^2$ and $\sigma_h = 2.5 \times 10^{-20} \text{ cm}^2$), affect the device performance - *contributes 100% with positive charge to N_{eff} at RT and has an insignificant contribution to LC at RT (~0.002% LC)*. This study revealed that the B_iO_i generation rate does not depend only on B, C and O content but also on the type of irradiating particles and fluence. For the same material, same doping and impurity content, the B_iO_i generation rate stays constant only for low hadron fluence, below 10^{11} cm^{-2} . The results presented in Fig.3 show that the B_iO_i introduction rate ($g_{B_iO_i}$) increases when the resistivity is lowered (as expected), is constant for medium resistivity and fluences below 10^{11} n/cm^2 : *For fluences above 10^{12} n/cm^2 $g_{B_iO_i}$ decreases and the determined values start to become un-reproducible even when re-measure the same sample.* Similar large “scattering” of the results is observed also in CV/IV or TSC electrical measurements and represent a major obstacle in controlling the acceptor removal process in the devices of interest.

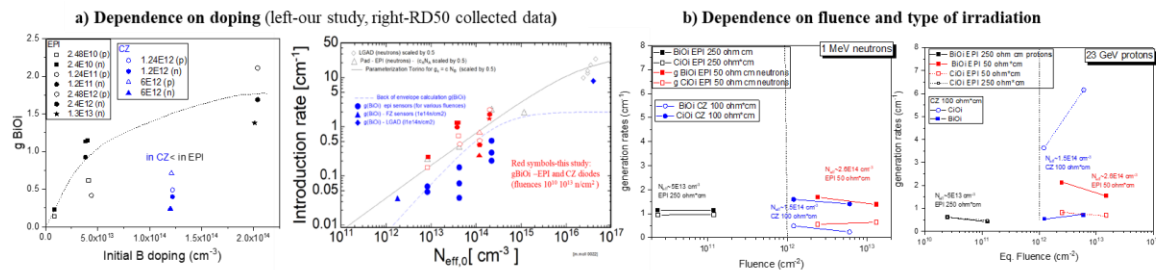
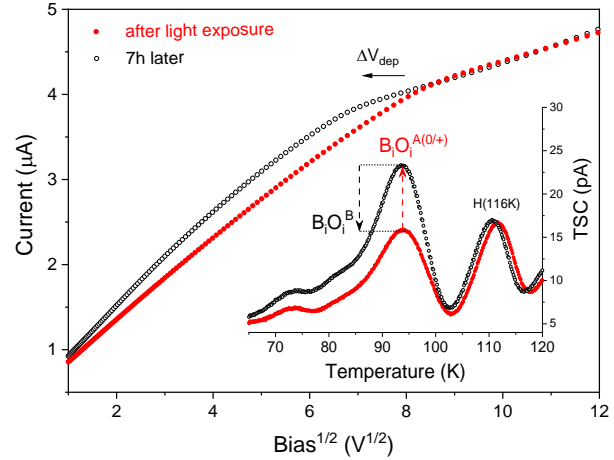


Fig. 3. Dependence of B_iO_i generation rate on: a) doping of DEPSIS diodes only (left) and on various diodes within RD50 (right); b) fluence and type of irradiation

- Metastability of B_iO_i defect. A special effort was dedicated to understand the reasons behind the large spread of the results obtained even when measuring the same sample, at the same annealing stage, affecting thus the evaluation of the acceptor removal process. We succeed demonstrating that the reason behind is that the B_iO_i defect has at least two configurations, A and B, of which only A

Fig. 4. TSC and IV for STFZ 4 k Ω cm and $\Phi=10^{15} \text{ n/cm}^2$, bistability of B_iO_i , 1st after exposing the samples to an excess of carriers prior to measurement and 2nd 7h later.



is detected in electrical measurements – see Fig.4.

We found that the variations in $[B_iO_i^A]$ are triggered by subjecting the samples to an excess of carriers, by either heating or an inherent short exposure to ambient light when manipulating the samples prior to experiments. Both, the $[B_iO_i^A]$ and N_{eff} , reach a steady state in ~ 7 hours. We expect that the magnitude of variations and time constants depend on the impurity content in the samples (Boron, Carbon, Oxygen), on the light intensity, on the damage status of the samples (e.g. Fermi level position in the bandgap, leakage current) and on temperature, and such dependencies shall be studied further. In addition, *as long as the amount of B_iO_i defects in the B configuration remains undetermined, a discrepancy in the estimations of Boron removal rates from CV/IV analyses and from defect spectroscopies will always exist, the smallest being achieved when all the measurements are performed on stabilized devices. The two configurations of the defect have a different impact on the acceptor removal rate g_B for both PAD and LGAD diodes ($g_B = 2 \times g_{B_iO_i^A} + g_{B_iO_i^B}$) and the defect balancing between the two is the main reason behind the large scattering of data.* The smallest discrepancy in the estimations of Boron removal rates between the results of CV/IV analyses and defect spectroscopies is achieved when all the measurements are performed on stabilized devices.

- Modelling of Coulombic centres: electric field approximations devoted to the 3D Poole-Frenkel (PF) emission from B_iO_i defects in the p-type region of the $n^{++}/p/p^{++}$ diodes. We started develop more complex theoretical models, accounting for the temperature and spatial variation of the electric field, so far considering only the B_iO_i defect (see Fig5a). For this defect, we determined the zero field activation energy (see Fig. 5b) and show that when the over-depletion is not properly accounted, the CV and TSC evaluations overestimate both the acceptor removal process and the generation rate of the B_iO_i defect. The variation of B_iO_i concentration, extracted from TSC, with the annealing temperature, depicted in Fig. 5c, was used to determine the activation energy and the frequency factor for annealing-out of the B_iO_i of $E_a = 1.35$ eV and $k_0 = 2,58 \times 10^{11} \text{ s}^{-1}$, respectively. *The increase of N_{eff} at temperatures above 150 °C correlates with the annealing-out of $B_iO_i^A(0/+)$, the change of N_{eff} being about two times the change of B_iO_i . This fact reflects that the B_iO_i dissociate, releasing B_i which turns into B_s , and that the defect initially in the B configuration is in considerable less concentration than in the A configuration (in stabilized devices).*

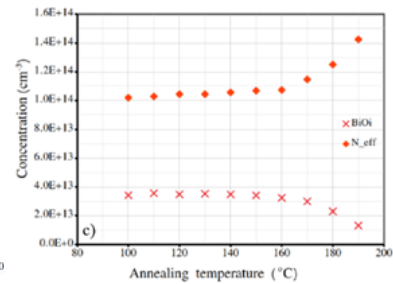
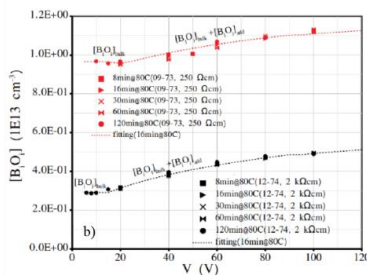
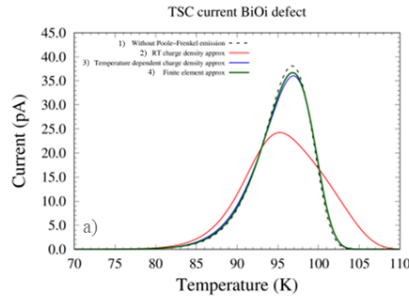


Figure 5: a) TSC current corresponding to a single PF type defect (BiO_i) in the 4 approximations; b) results of TSC measurements for quantifying the PF effect in the case of BiO_i ; c) dependence of N_{eff} (from C-V) and $[\text{BiO}_i]$ (from TSC) on the isochronal annealing temperature for an EPI- 50 Ωcm diode irradiated with 23 GeV protons, $\Phi_{\text{eq}} = 4.3 \times 10^{13} \text{ cm}^{-2}$

Among the obtained results the most relevant ones for the scientific community are related to:

(i) the BiO_i defect, which proved to be the main cause for both, the acceptor removal process in p-type silicon and the unusual large scattering of the data which can be now justified by a valid physical explanation - the bistable nature of the defect. We detected up to 100% variations in $[\text{BiO}_i^A]$ in first 7h from exposure of the sample to laboratory ambient light - meaning that, during this time, a considerable amount of BiO_i is "hidden" in yet undetected B configuration, being thus not accounted when calculating the defect generation rate. The correct BiO_i generation rate should include the amount in the yet undetected B configuration ($g_{\text{BiO}_i} = g_{\text{BiO}_i^A} + g_{\text{BiO}_i^B}$); The smallest discrepancy in the estimations is achieved when all the measurements are performed on stabilized devices.

(ii) the amount of Boron in the investigated samples. This was detected in LA-ICPMS experiments to be in much larger concentrations than expected from the data provided by wafers suppliers. Depending on the producer, it can be up to 100 times larger, due to a not-specified compensation with Phosphorous. Such discrepancies has a tremendous impact for any attempt of parametrizing the acceptor removal process in Boron doped silicon. Future experiments must account for the real concentration of Boron atoms and not rely on the assumption that the vendors use only B as dopant.